ACTA IMEKO
ISSN: 2221-870X
December 2023, Volume 12, Number 4, 1 - 6

Modeling and simulation of dew point temperature generated by a bubble aerator

Arfan Sindhu Tistomo[1,2], Aditya Achmadi[2], Melati Azizka Fajria[2], Sparisoma Viridi[3], M. Miftahul Munir[3], S. Suprijadi[3]

[1] *Doctoral Program of Physics, Faculty of Mathematics and Natural Science, Institut Teknologi Bandung, Bandung, Indonesia*
[2] *National Measurement Standards, National Standardization Agency of Indonesia, Banten, Indonesia*
[3] *Department of Physics, Faculty of Mathematics and Natural Science, Institut Teknologi Bandung, Bandung, Indonesia*

ABSTRACT
The dew point temperature can be generated by saturating air with water vapor through several methods, one of which is by creating small-sized air bubbles passed through water in an enclosed space known as a saturator. In practical terms, the dew point temperature produced by this system can be determined by measuring it using a dew point meter. However, the prediction of the dew point temperature generated through theoretical approaches has not been presented before. Thus, in this study, a simulation has been conducted to determine the dew point temperature. The result is then compared to the experimental data. The experiment follows the single pressure humidity generator principle, where a saturator containing a bubble aerator is immersed in a stirred liquid bath. The bath temperature is set to 25 °C, and the gas flow rate is adjusted from 0.1 lpm to 0.4 lpm. The dew point temperature is measured using a 373 LHX chilled mirror dew point meter. On the other hand, the simulation is performed using the Monte Carlo method, and the physical model involves a heat balance between convection and the change in bubble energy. The convection heat transfer coefficient is determined by the behavior of bubble dynamics, which is related to the bubble size and bubble velocity. The dew point temperature obtained from the simulation is assumed to be the same as the bubble temperature. As a result, the simulation data align well with the experimental data.

Section: RESEARCH PAPER

Keywords: Dew point; temperature; Monte Carlo; humidity; bubble; aerator; applied mathematics

Citation: Arfan Sindhu Tistomo, Aditya Achmadi, Melati Azizka Fajria, Sparisoma Viridi, M. Miftahul Munir, S. Suprijadi, Modeling and simulation of dew point temperature generated by a bubble aerator, Acta IMEKO, vol. 12, no. 4, article 44, December 2023, identifier: IMEKO-ACTA-12 (2023)-04-44

Section Editor: Laura Fabbiano, Politecnico di Bari, Italy

Received May 2, 2023; **In final form** December 11, 2023; **Published** December 2023

Funding: Indonesia Endowment Fund for Education (Lembaga Pengelola Dana Pendidikan-LPDP) and RISPRO LPDP

Corresponding author: Arfan Sindhu Tistomo, e-mail: tistomo2020@gmail.com

1. INTRODUCTION

Dew point temperature is one of the quantities used to express the amount of water vapor in the air (humidity). In most cases, the dew point temperature is used to establish traceability for hygrometers to the International System of Units (SI) through a primary reference called a dew point generator. Normally, a dew point generator consists of a saturator chamber that saturates the air with water vapor, resulting from the thermodynamic equilibrium between the gas and liquid phases of water at a certain temperature (*Ts*) and pressure (*Ps*). As a result, the saturation water vapor as a function of Ts and Ps can be calculated [1], [2] and other humidity quantities such as relative humidity can be linked.

Saturator design is the key to achieving 100 % saturation. Several types of saturators have been reported: coil type [3]-[7], box vessel or chamber type followed by a heat exchanger [8]-[10], labyrinth type [11], and bubble type [12].

Currently, the study of air bubbles flowing in a solution, including pure water, is of great interest. Particularly, the investigation of bubble velocity, referred to as rise or terminal velocity (U_b) has been prominent. In most cases, this velocity is a function of the bubble size (D_b) [13]-[17]. A concise representation of their relationship has been graphically reported [18], [19]. Consequently, many researchers have formulated equations to calculate terminal velocity using this data [20]-[23].

In this study, a model is developed and simulated for the dew point generated by a bubble aerator. The model is based on heat

transfer principles, while the simulation employs the Monte Carlo method. This method has emerged as a potent tool for both assessing measurement uncertainty and enhancing accuracy [24]-[31], following the publication of its guidelines [32]. This method is able to accommodate fluctuations in input parameters, thus approximating real conditions. In addition, the output of this method is presented in the form of a histogram, which can be statistically analysed. After obtaining the results, they are then compared to experimental data.

2. METHOD

2.1. Modelling

The energy balance between the bubble and the water or its surroundings in the saturator occurs when the heat transferred into the bubble during *dt* is equal to the increase in the bubble's energy during *dt*. The mathematical model is as follows:

$$hA_s(T_s - T)dt = mC_p dT\,, \tag{1}$$

where h is the convection heat transfer coefficient, A_s is the surface area through which convection heat transfer takes place, m is the mass of the bubble, C_p is the specific heat at constant pressure. Since $m = \rho V$ (ρ is the bubble density, V is the bubble volume), $dT = d(T - T_s)$, and T_s does not fluctuate much, the equation (1) can be rearranged as

$$\frac{d(T - T_s)}{T - T_s} = -\frac{\mathrm{h\,A_s}}{\rho\, V\, C_p}dt, \tag{2}$$

By integration, the final equation is as follows

$$\frac{T(t) - T_s}{T_i - T_s} = \mathrm{e}^{-jt}\,, \tag{3}$$

where T_i is the initial temperature and $j = \frac{hA_s}{\rho V C_p}$. The dew point temperature (T_d) is equal to the bubble temperature $T(t)$. The convection heat transfer coefficient h is obtained using Nusselt number as follows [33]

$$h = \frac{Nu\, k_l}{D_b}, \tag{4}$$

$$Nu = 2 + \left(0.4\, Re^{0.5} + 0.06\, Re^{\frac{2}{3}}\right) Pr^{0.4}\,, \tag{5}$$

$$Re = \frac{\rho_l\, U_b\, D_b}{\mu_l}\,, \tag{6}$$

$$Pr = \frac{C_p\, \mu_l}{k_l}\,, \tag{7}$$

Nu is the Nusselt number, Re is the Reynolds number, Pr is the Prandtl number, ρ_l is the water density, μ_l is the water viscosity, and k_l is the water thermal conductivity.

According to Mendelson [20] there are four regions related to bubble behaviour. Region 1 is defined when the bubble size has a diameter less than 0.07 cm. In this region, the terminal velocity is limited by viscous drag and follows the Stokes law. In Region 2, bubbles have a diameter between 0.07 cm and 0.14 cm. Although the terminal velocity is also constrained by viscosity, it surpasses what Stokes law predicts due to internal circulation within the bubble. Region 3 encompasses bubble diameters between 0.14 cm and 0.6 cm. Bubbles in this range are no longer spherical and tend to follow zigzag or helical paths. Region 4 covers bubble diameters above 0.6 cm, where bubbles begin to assume a spherical cap shape.

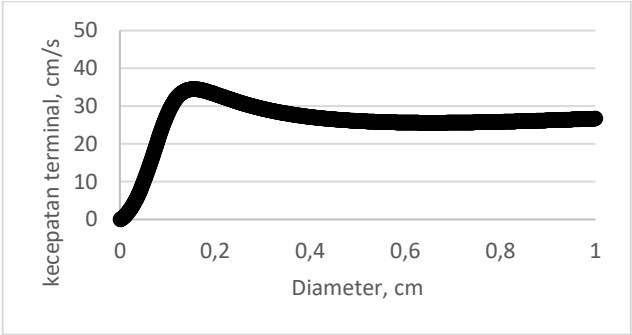

Figure 1. Bubble terminal velocity plotted using (8).

Among the various terminal velocity formulations, this study opts for the formula proposed by S. Baz- follows [33] due to its good fit with experimental data, while some others are only suitable for specific regions. The terminal velocity can be expressed as follows:

$$U_b = \frac{1}{\sqrt{\frac{1}{U_1^2} + \frac{1}{U_2^2}}}, \tag{8}$$

$$\mathrm{U_1} = U_{pot}\left[1 + 0.73667\frac{(gD_b)^{\frac{1}{2}}}{U_{pot}}\right]^{\frac{1}{2}}, \tag{9}$$

$$U_{pot} = \frac{1}{36}\frac{g\, D_b^2(\rho_l - \rho)}{\mu_l}, \tag{10}$$

$$U_2 = \left(\frac{3\sigma}{\rho_l D_b} + \frac{gD_b(\rho_l - \rho)}{2\rho_l}\right)^{1/2}, \tag{11}$$

g is the acceleration of gravity, μ_l is the dynamic viscosity of the water, and σ is the surface tension. The profile of the terminal velocity can be seen in Figure 1.

2.2. Simulation

The Monte Carlo Simulation is based on the propagation of distributions. If there is a function $y = f(x_1, x_2, x_3)$ then the value of y, along with its associated uncertainty, can be estimated through the distribution of the input quantities x_1, x_2, x_3 as illustrated in Figure 2.

Therefore, based on the modelling scheme, the distributions of bubble size, bubble density, and saturation temperature should

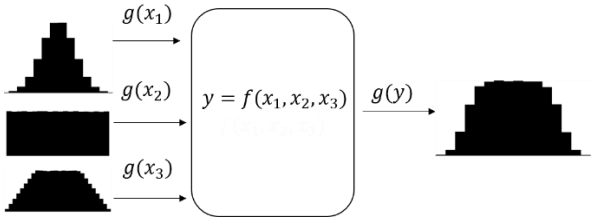

Figure 2. Illustration of the Monte Carlo simulation, where $g(x_1), g(x_2), g(x_3)$ are the distribution functions of the input quantities and $g(y)$ is the distribution function of the measurand.

Table 1. The uncertainty components for P_s.

Source of the uncertainty of P_s	Distribution	Standard uncertainty
Calibration	Normal	250 Pa
Drift	Uniform	130 Pa
Resolution	Uniform	0.5 Pa
Repeatability	Normal	35 Pa

be known. The simulation is executed using R Statistics and Python, generating 1,000,000 random numbers. Once the bubble size is determined, the bubble density can be estimated using the equation below:

$$\rho = ((P_s + \rho_l g h_d) + \frac{2s}{r}) \times \frac{28}{R_g T_i} \quad , \tag{12}$$

where h_d is the bubble depth, s is the surface tension, R_g is the gas constant, r is the bubble radius. The saturation pressure P_s has uncertainty components listed in Table 1, where the repeatability is determined by the highest value among the gas flow rate setups.

In order to maintain the saturator temperature relatively constant, the saturator is immersed in a stirred bath as will be discussed in the experimental work. Consequently, the initial bubble temperature is approximated to be equal to the bath temperature. Therefore, its uncertainty component is listed in Table 2.

Accurate measurement of the depth (h_d) presents challenges due to potential changes in the water surface caused by evaporation. As a result, it is estimated to be 7 cm, with a standard uncertainty of 0.5 cm, and follows a uniform distribution.

2.3. Experimental Work

To obtain the terminal velocity, the bubble size needs to be determined using equation (8). As such, an experimental setup was devised. The bubble aerator was positioned within a transparent chamber filled with water. An air pump, coupled with a flowmeter, generated the airflow, adjusted to 0.1 lpm, 0.2 lpm, 0.3 lpm, and 0.4 lpm. A camera operating at a speed of 50 fps captured images of the bubbles formed by the aerator. Utilizing the software JImage [35], the bubble's shape was fitted to an elliptical model, allowing for calculation of the bubble diameter using the following equation:

$$D_b = \sqrt[3]{(2a)^2 \times (2b)}\,, \tag{13}$$

where a and b are the major and minor semi-axes of an ellipse, respectively. For each speed of air, the distribution of the bubble diameter is estimated.

Subsequently, the bubble aerator was placed inside a stainless steel jar at a depth of 7 cm. Serving as the saturator chamber, the jar possessed dimensions of 11 cm in diameter and 15.5 cm in height. During the dew point measurement, the saturator connected to a stainless steel heat exchanger with an outer diameter of 10 mm, inner diameter of 8 mm, and length of 6 m. The heat exchanger was used to ensure that the gas temperature equilibrated with the bath temperature upon entry into the saturator, as depicted in Figure 3.

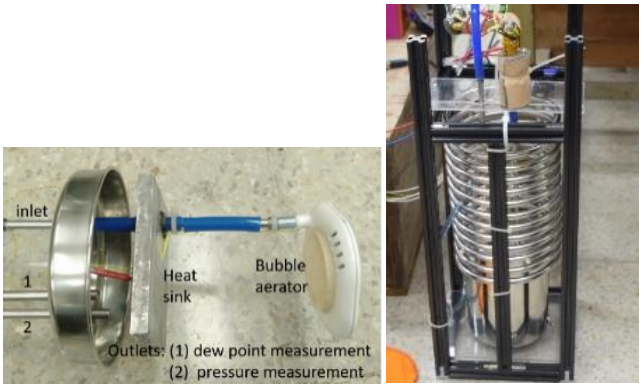

Figure 3. The saturator. Heatsink is used to block water splash caused by bubble movement.

A chilled mirror dew point meter, model 373 by RHSystems, was linked to one of the outlets for dew point measurement. Pressure measurement was conducted by connecting the pressure outlet to the atmospheric pressure port at the rear of the device. The bath temperature was set to 25°C, and the airflow was adjusted to 0.1 lpm, 0.2 lpm, 0.3 lpm, and 0.4 lpm. As the dew point temperature exceeded room temperature, the outlet gas line was heated to 25°C above the dew point temperature to prevent condensation within the pipe.

3. RESULTS AND DISCUSSION

3.1. Bubble Distribution

The bubble size distribution is derived from the bubble size measurements by creating a histogram from the collected data. Unfortunately, the shape does not follow a Gaussian distribution but rather closely resembles the Gamma distribution. Through trial-and-error simulations, a gamma function was established to generate random numbers that replicate the bubble size distribution. The Gamma formulation for each gas flow rate is provided in Table 3, and an example of the histogram comparison between the original data and the simulation at 0.1 lpm is illustrated in Figure 4.

3.2. Terminal Velocity

At a bath temperature of 25 °C, the saturation pressure measurements for each gas flow rate are presented in Table 4. While the saturation pressures vary with each gas flow rate, the

Table 2. The uncertainty components for T_i.

Source of the uncertainty of T_i	Distribution	Standard uncertainty
Sensor calibration	Normal	0.015 °C
Sensor drift	Uniform	0.01/ √3 °C
Self-heating	Uniform	0.005/√3 °C
Repeatability	Normal	0.004 °C
Bridge Calibration	Normal	0.01 °C
Bath stability	Uniform	0.02 /√3 °C
Bath uniformity	Uniform	0.05 /√3 °C

Table 3. The Gamma formulation for each gas flow rate. The code is in R language.

Gas Flow Rate	Random Variable	Diameter Formulation
0.1 lpm	r_1=runif(10^6, 0,2) r_2=runif(10^6,1,2)	$D_b = -\frac{\ln(r_1 \times r_2)}{2.5} + 0.798$
0.2 lpm	r_1=runif(10^6, 0,1) r_2=runif(10^6,0,1)	$D_b = -\frac{\ln(r_1 \times r_2)}{2.7} + 0.275$
0.3 lpm	r_1=runif(10^6, 0,1) r_2=runif(10^6,0,1)	$D_b = -\frac{\ln(r_1 \times r_2)}{2.93} + 0.31$
0.4 lpm	r_1=runif(10^6, 0,1) r_2=runif(10^6,0,1)	$D_b = -\frac{\ln(r_1 \times r_2)}{2.63} + 0.209$

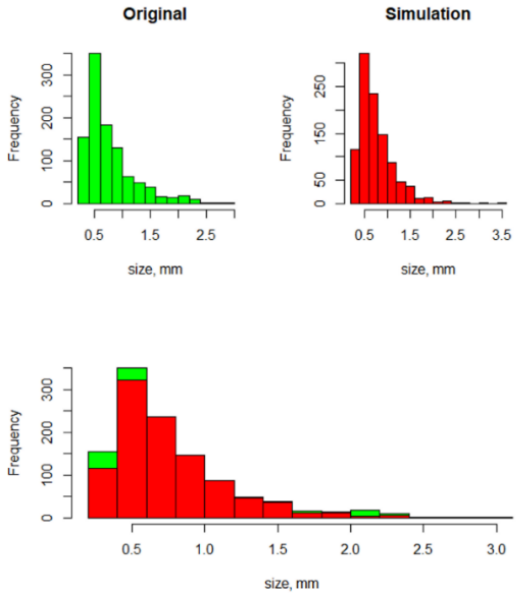

Figure 4. Histogram comparison between original data and simulation at 0.1 lpm. The bottom graph shows the two histograms plotted in a single frame.

Table 4. Saturation pressure measurement.

Gas Flow Rate	Saturation pressure P_s
0.1lpm	100172 Pa
0.2 lpm	100106.2 Pa
0.3 lpm	100105.2 Pa
0.4 lpm	100094.5 Pa

difference between the highest and the lowest values remains within the calibration uncertainty. This suggests that the variation is due to the stability of the pressure transducers rather than fluctuations in pressure within the saturator.

When combined with the bubble size distribution, the terminal velocity for each gas flow rate setup can be graphed, as depicted in Figure 5. It is evident that larger bubbles are produced with higher gas flow rates.

3.3. Dew Point Temperature

The dew point temperature, as measured by the chilled mirror dew point meter, is presented in Figure 6. It's evident that a stable state of dew point temperature cannot be observed when the gas

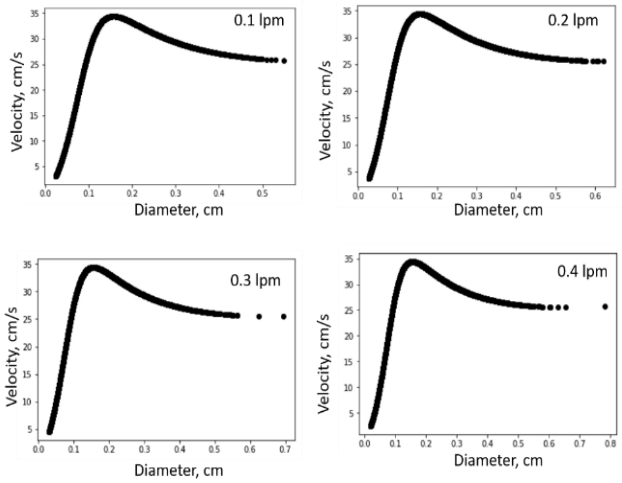

Figure 5. Terminal velocity for each gas flow rate.

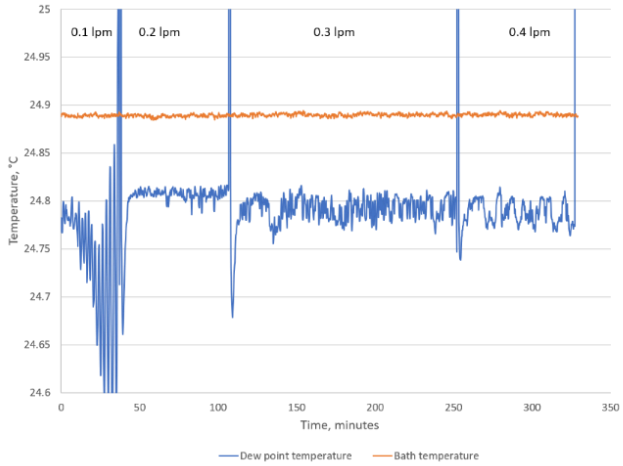

Figure 6. Dew point temperature measurement using 373 chilled mirror dew point meter.

flow rate is set to 0.1 lpm. This behaviour could potentially result from the gas flow entering the device falling short of requirements. Moreover, it appears that our chilled mirror dew point meter exhibits flow dependence, as evidenced by the dew point temperature at a gas flow rate of 0.2 lpm being slightly higher than that at 0.3 lpm and 0.4 lpm.

For the purpose of comparison with simulation results, the average and standard deviation are calculated, alongside uncertainty components from resolution ($0.005/\sqrt{3}$°C) and calibration (0.11/2 °C). This information is used to construct the histogram of experimental data."

From the experimental data, the parameters needed to run the simulation based on equation (3) are obtained. Notably, the saturator temperature is never higher than the initial bubble temperature, which is assumed to be the bath temperature. The average bath temperature is Ti = 24.89 °C. As a result, the estimated saturator temperature Ts is Ti - 0.1 °C, considering the relatively large volume of the jar. The time 't' is set to 0.5 s to ensure that the bubble reaches its terminal velocity. Dew point temperatures for all gas flow rates are consistent, with a value of 24.790 °C ± 0.071 °C at a 95% confidence level. A comparison with the experimental data is presented in Figure 7.

It can be observed that both histograms have the same average value but different standard deviations. However, according to ISO 13528 [36], the En number can be calculated and is found to be 0 or less than 1. As a result, the comparison result is satisfactory.

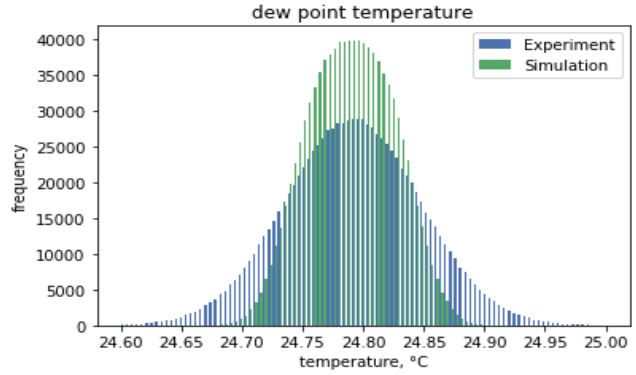

Figure 7. Comparison between simulation and experiment.

4. CONCLUSIONS

The dew point temperature generated by a bubble aerator can be accurately predicted through simulation using a physical model based on heat balance between convection and the change in bubble energy. In this simulation, the dew point temperature is simply equal to the bubble temperature. The dynamics of the bubble, particularly its size and velocity, play a significant role in the thermodynamic equilibrium within the saturator. For instance, an experiment to measure the dew point temperature at 25 °C is conducted using the single pressure humidity generator principle, and the simulation yields the same value with better uncertainty evaluation using the Monte Carlo method.

In contrast to the simulation, the experimental data exhibits gas flow rate dependency. At 0.1 lpm, the dew point temperature cannot stabilize, and at 0.2 lpm, the measured dew point temperature is higher than the others.

A challenge for the simulation lies in accurately estimating the saturator temperature (*Ts*). In this study, *Ts* is approximated to be 0.1 °C below the bath temperature, but this may vary for other dew point temperature measurements and saturator volumes. The best approach is to directly measure the water temperature inside the saturator using an identical sensor employed for measuring the bath temperature. As a result, this improvement will be undertaken in the near future.

ACKNOWLEDGEMENT

We express gratitude to the Indonesia Endowment Fund for Education (Lembaga Pengelola Dana Pendidikan-LPDP) and RISPRO LPDP for the financial support.

REFERENCES

[1] B. Hardy, ITS-90 formulations for vapor pressure, frostpoint temperature, dewpoint temperature, and enhancement factors in the range–100 to+ 100 C, Proc. of the Third Int. Symp. on Humidity & Moisture, 1998, pp. 1–8.

[2] D. Sonntag, Important new values of the physical constants of 1986, vapour pressure formulations based on the ITS-90, and psychrometer formulae, Zeitschrift für Meteorologie, vol. 40, no. 5, pp. 340–344, 1990.

[3] H. Liedberg, M. Mnguni, D. Jonker, A simple humidity generator for relative humidity calibrations, Int. Journal of Thermophysics, vol. 29, no. 5, pp. 1660–1667, 2008.
DOI: 10.1007/s10765-008-0423-z

[4] D. Zvizdic, T. Stasic, L. G. Bermanec, Characterization of LPM'S 1-T dew point generator, in IMEKO World congress, Rio de Janeiro, Brazil, 17-22 September 2006. Online [Accessed 19 December 2023] https://www.imeko.org/publications/wc-2006/PWC-2006-TC12-022u.pdf

[5] R. Bosma, A. Peruzzi, Development of a dew-point generator for gases other than air and nitrogen and pressures up to 6 MPa, International Journal of Thermophysics, vol. 33, 2012, no. 8, pp. 1511-1519.
DOI: 10.1007/s10765-012-1214-0

[6] C. FitzGerald, D. Mac Lochlainn, R. Strnad, N. Hodžić, Development of a new primary humidity measurement standard, Measurement Science and Technology, vol. 31, 2019, no. 2, p. 024007.
DOI: 10.1088/1361-6501/ab4a54

[7] D. Hudoklin, J. Drnovšek, The New LMK Primary Standard for Dew-Point Sensor Calibration: Evaluation of the High-Range Saturator Efficiency, Int J Thermophys, vol. 29, no. 5, Oct. 2008, pp. 1652–1659.
DOI: 10.1007/s10765-007-0367-8

[8] D. Zvizdic, M. Heinonen, D. Sestan, New Primary Dew-Point Generators at HMI/FSB-LPM in the Range from −70 °C to +60 C, Int J Thermophys, vol. 33, no. 8–9, Sep. 2012, pp. 1536–1549.
DOI: 10.1007/s10765-012-1211-3

[9] H. Sairanen, M. Heinonen, R. Högström, J. Salminen, S. Saxholm, H. Kajastie, Low-pressure and low-temperature dew/frost-point generator, International Journal of Thermophysics, vol. 39, no. 9, 2018, p. 104.
DOI: 10.1007/s10765-018-2425-9

[10] S. Oğuz Aytekin, N. Karaböce, M. Heinonen, H. Sairanen, A New Primary Dew-Point Generator at TUBITAK UME, Int J Thermophys, vol. 39, no. 5, May 2018, p. 62.
DOI: 10.1007/s10765-018-2375-2

[11] H. Mitter, New BEV/E+E Elektronik Low-Frost-Point/High-Pressure Generator, Int J Thermophys, vol. 36, no. 8, Aug. 2015, pp. 2242–2258.
DOI: 10.1007/s10765-015-1950-z

[12] R. Bosma, J. Nielsen, A. Peruzzi, Development of the High-Temperature Dew-Point Generator Over the Past 15 Years, Int J Thermophys, vol. 38, no. 10, Oct. 2017, p. 161.
DOI: 10.1007/s10765-017-2291-x

[13] H. Ivey, Relationships between bubble frequency, departure diameter and rise velocity in nucleate boiling, International Journal of Heat and Mass Transfer, vol. 10, no. 8, 1967, pp. 1023–1040.
DOI: 10.1016/0017-9310(67)90118-4

[14] M. A. Talaia, Terminal velocity of a bubble rise in a liquid column, World Academy of Science, Engineering and Technology, vol. 28, 2007, pp. 264–268.
DOI: 10.5281/zenodo.1070173

[15] L. Liu, H. Yan, G. Zhao, J. Zhuang, Experimental studies on the terminal velocity of air bubbles in water and glycerol aqueous solution, Experimental Thermal and Fluid Science, vol. 78, 2016, pp. 254–265.
DOI: 10.1016/j.expthermflusci.2016.06.011

[16] A. Battistella, S. van Schijndel, M. Baltussen, I. Roghair, M. van Sint Annaland, On the terminal velocity of single bubbles rising in non-Newtonian power-law liquids, Journal of Non-Newtonian Fluid Mechanics, vol. 278, 2020, p. 104249
DOI: 10.1016/j.jnnfm.2020.104249

[17] P. A. Suriasni, F. Faizal, C. Panatarani, W. Hermawan, I. M. Joni, A Review of Bubble Aeration in Biofilter to Reduce Total Ammonia Nitrogen of Recirculating Aquaculture System, Water, vol. 15, no. 4, 2023, p. 808.
DOI: 10.3390/w15040808

[18] W. L. Haberman, R. K. Morton, An experimental investigation of the drag and shape of air bubbles rising in various liquids, David Taylor Model Basin Washington DC, 1953.

[19] F. Peebles, H. Garber, Studies on the motion of gas bubbles in liquid, Chem. Eng. Prog., 49, 1953, n. 2, pp. 88-97.

[20] H. D. Mendelson, The prediction of bubble terminal velocities from wave theory, AIChE Journal, vol. 13, 1967, no. 2, pp. 250-253.
DOI: 10.1002/aic.690130213

[21] F. Raymond, J.-M. Rosant, A numerical and experimental study of the terminal velocity and shape of bubbles in viscous liquids, Chemical Engineering Science, vol. 55, 2000, no. 5, pp. 943–955.
DOI: 10.1016/S0009-2509(99)00385-1

[22] G. Bozzano, M. Dente, Shape and terminal velocity of single bubble motion: a novel approach, Computers & chemical engineering, vol. 25, 2001, no. 4–6, pp. 571–576.
DOI: 10.1016/S0098-1354(01)00636-6

[23] E. Michaelides, Particles, bubbles & drops: their motion, heat and mass transfer. World Scientific, 2006.

[24] H. Sato, Influence of index table accuracy on roundness calibration in the multi-step method using monte carlo simulation, Mapan, vol. 26, 2011, no. 1, pp. 37–46.
DOI: 10.1007/s12647-011-0004-7

[25] G. Moona, V. Kumar, M. Jewariya, R. Sharma, H. Kumar, Measurement uncertainty evaluation using Monte Carlo

simulation for newly established line scale calibration facility at CSIR-NPLI, MAPAN, vol. 34, 2019, no. 3, pp. 325–331. DOI: 10.1007/s12647-019-00327-7

[26] S. Rab, S. Yadav, A. Zafer, A. Haleem, P. K. Dubey, J. Singh, R. Kumar, R. Sharma, L. Kumar, Comparison of Monte Carlo simulation, least square fitting and calibration factor methods for the evaluation of measurement uncertainty using direct pressure indicating devices, Mapan, vol. 34, 2019, no. 3, pp. 305–315. DOI: 10.1007/s12647-019-00333-9

[27] A. S. Tistomo, D. Larassati, A. Achmadi, Purwowibowo, G. Zaid, Estimation of uncertainty in the calibration of industrial platinum resistance thermometers (iprt) using monte carlo method, Mapan, vol. 32, 2017, no. 4, pp. 273–278. DOI: 10.1007/s12647-017-0222-8

[28] I. P. Aronov, P. M. Aronov, E. P. Sobina, Increasing the Accuracy of Measurements of Absolute Gas Permeability by a Stationary Filtration Method, Measurement Techniques, 2022, pp. 1–9. DOI: 10.1007/s11018-022-02105-5

[29] V. Isaiev, O. Velychko, Metrological characterisation of current transformers calibration unit for accurate measurement, Acta IMEKO, vol. 10, 2021, no. 2, pp. 6–13. DOI: 10.21014/acta_imeko.v10i2.918

[30] C. Wuethrich S. Souiyam, Monte Carlo determination of the uncertainty of effective area and deformation coefficient for a piston cylinder unit, Acta IMEKO, vol. 9, 2020, no. 5, pp. 338–342. DOI: 10.21014/acta_imeko.v9i5.996

[31] N. Morresi, S. Casaccia, M. Arnesano, G. M. Revel, Impact of the measurement uncertainty on the monitoring of thermal comfort through AI predictive algorithms, Acta Imeko, vol. 10, 2021, no. 4, pp. 221–229. DOI: 10.21014/acta_imeko.v10i4.1181

[32] J. JCGM, "101: 2008 Evaluation of measurement data–supplement 1 to the 'guide to the expression of uncertainty in measurement'–propagation of distributions using a Monte Carlo method," International Organisation for Standardisation, Geneva, 2008.

[33] S. Whitaker, Forced convection heat transfer correlations for flow in pipes, past flat plates, single cylinders, single spheres, and for flow in packed beds and tube bundles, AIChE Journal, vol. 18, 1972, no. 2, pp. 361–371. DOI: 10.1002/aic.690180219

[34] S. Baz-Rodríguez, A. Aguilar-Corona, A. Soria, Rising velocity for single bubbles in pure liquids, Revista mexicana de ingeniería química, vol. 11, no. 2, pp. 269–278, 2012.

[35] Fiji distribution of ImageJ website. Online [Accessed] https://imagej.net/software/fiji/downloads

[36] International Organization for Standardization (ISO), "ISO 13528 (2015) Statistical methods for use in proficiency testing by interlaboratory comparisons." International Organization for Standardization (ISO), Geneva.